2024, 21(5): 1625-1638
https://dx.doi.org/10.21123/bsj.2023.8312
P-ISSN: 2078-8665 - E-ISSN: 2411-7986
Baghdad Science Journal

The effect of heat transformation and rotation on Sutterby fluid peristaltic flow in an inclined, asymmetric channel with the porousness

***Asmaa A. Mohammed* [*1,2], *Liqaa Zeki Hummady* [1]**

Department of Mathematics, College of Science, University of Baghdad, Baghdad, Iraq
Department of Mathematics, College of Science for Women, University of Baghdad, Baghdad, Iraq
*Corresponding Author.

Received 01/01/2023, Revised 24/03/2023, Accepted 26/03/2023, Published Online First 20/10/2023, Published 01/05/2024

Abstract

In this paper, the effect of the rotation variable and other variables on the peristaltic flow of Sutterby fluid in an Inclined asymmetric channel containing a porous medium with heat transfer is examined. In the presence of rotation, mathematical modeling is developed using constitutive equations based on the model of Sutterby fluid. In flow analysis, assumptions such as long wavelength approximation and low Reynolds number are used. The resulting nonlinear ordinary differential equation was analytically solved using the perturbation method. The effects of the Grashof number, the Hartmann number, the Reynold number, the Froude number, the Hall parameter, the Darcy number, the magnetic field, the Sutterby fluid parameter, and heat transfer analysis on the stream function, and the pressure gradient are analyzed graphically. Utilizing MATHEMATICA software, numerical results were computed. It is discovered that the size of boluses decreases as some parameters increase, whereas the pressure gradient is directly proportional to the majority of parameters.

Keywords: Heat transform, Magnetic field, Peristaltic flow, Porousness, Sutterby fluid.

Introduction

Peristaltic pumping is a special type of pumping when it is simple to transport a variety of complex rheological fluids from one location to another. This pumping principle is referred to as peristaltic [1]. Some examples of such physiological processes are the passage of food, chyme, and urine. Peristalsis is the driving force behind everything from worm movement to the transfer of noxious and clean fluids to the operation of finger pumps and the heart-lung machine. Damping, dispensability, and tension in the vasculature play a critical part in physiological processes involving peristalsis, such as blood flow [2]. Studies of peristalsis were first introduced [3, 4]. Since then, researchers have made numerous attempts to dissect the peristaltic movement of fluids and its implications in the medical and business worlds. In biological systems and industrial fluid transport, heat transfer is a fundamental principle. One of the most essential roles of the cardiovascular system is maintaining the body's temperature. Air that enters the lungs must also be tempered to the body's temperature. This is accomplished through the use of all blood vessels. There are three methods of heat transmission;

2024, 21(5): 1625-1638
https://dx.doi.org/10.21123/bsj.2023.8312
P-ISSN: 2078-8665 - E-ISSN: 2411-7986
Baghdad Science Journal

however, convection is the most relevant for fluid circulation in the human body. Human and animal bodies use convection heat transfer to release heat generated by metabolic processes into the environment [1]. In recent years, the effects of changing viscosity, heat transfer, and mass transfer on magnetohydrodynamic (MHD) peristaltic flow in an asymmetric tapering inclined channel with porous material were Examined [5]. A hybrid nanoflow of Casson fluid was addressed. The theoretical formulation is derived by considering spherical and, as well as, platelet shape nanoparticles. Electro-osmotic flow (EOF) through an asymmetric channel endures the simultaneous effects of Joule heating, viscous dissipation and magnetic fields [6].

For a high magnetic field like in MHD flows, hall current has significant effects. This phenomenon is widely used in a variety of fields, including the design of power generators, Hall accelerators, refrigeration coils, electric transformers, and spacecraft propulsion systems. The peristaltic transport in the presence of Hall current has been the subject of several published works. The effect of Hall current, viscosity variation, and porous medium on the peristaltic transport of viscoelastic fluid through irregular microchannels was studied [6]. The effect of magnetohydrodynamic (MHD) on a viscous fluid generalized burgers' fluid with a gradient constant pressure and an exponentially accelerating plate, where the no-slip hypothesis between the burgers' fluid and the exponential plate is no longer applicable, were studied [7].

Since Abdulhadi [8], and Sadaf [9] examined the mechanism of peristaltic transport, it has attracted the interest of numerous researchers. Viscous liquids are less prevalent in industrial and physiological processes than non-Newtonian fluids. Shampoo, ketchup, lubricants, paints, and blood are all examples of non-Newtonian substances found in nature. Among that, Sutterby liquid [10] is one of the materials that characterize ionic high polymer solutions. Convection and Hall current were used to simulate the MHD peristaltic transport of a Sutterby nanofluid [11]. Waveform motion of non-Newtonian fluids through porous channels is discussed [12, 13], where the effects of rotation and an inclined MHD are considered. Magnetohydrodynamic (MHD) for Williamson fluid with variable temperatures and variable concentrations in a slanted channel with variable viscosity has been investigated [14]. The effects of radiation and convection in a Sutterby fluid are discussed [15]. In Ramesh [16], electroosmotic peristaltic transport of Sutterby nanofluids is investigated. The peristaltic flow of a Sutterby liquid in an inclined channel was investigated [17].

In this paper, the study will look at the effects of rotation on heat transfer for peristaltic transport in an inclined asymmetric channel with a porous medium. This will be done by using different values of the parameters of rotation, amplitude wave, and channel taper, as well as different values of the Grashof number, the Hartmann number, the Reynold number, the Froude number, the Hall parameter, the Darcy number, the magnetic field, the Sutterby fluid parameter, and heat transfer analysis, based on the changes in stream function and pressure gradient.

Materials and Methods

A mathematical formulation for asymmetric flow

Consider the peristaltic transport of an incompressible Sutterby fluid through a two-dimensional asymmetric conduit that has a width of $(d' + d)$. whereas motion is constant within a coordinate system pumped at wave speed (c) in the wave framer $(\bar{X}, \bar{Y})$ as shown in

2024, 21(5): 1625-1638
https://dx.doi.org/10.21123/bsj.2023.8312
P-ISSN: 2078-8665 - E-ISSN: 2411-7986
Baghdad Science Journal

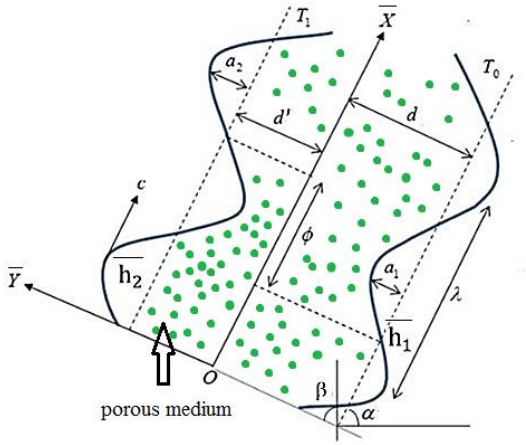

Figure 1.

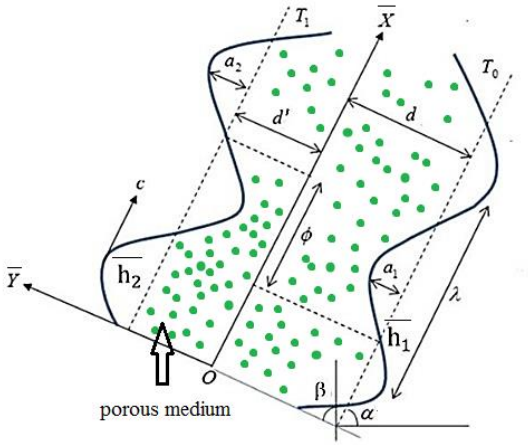

Figure 1. An inclined asymmetric channel coordinates in the Cartesian and Dimensional Systems with porous medium

The geometry of a wall's structure is described as:

$$\overline{h_1}(\bar{X},\bar{t}) = d - a_1 \sin\left[\frac{2\pi}{\lambda}(\bar{x} - c\bar{t})\right]. \quad 1$$

$$\overline{h_2}(\bar{X},\bar{t}) = -d' - a_2 \sin\left[\frac{2\pi}{\lambda}(\bar{x} - c\bar{t}) + \phi\right]. \quad 2$$

In which $\overline{h_1}(\bar{X},\bar{t})$, $\overline{h_2}(\bar{X},\bar{t})$ are the upper and lower wall respectively, (d, d') indicates the channel width, (a_1, a_2) are the wave's amplitudes, (λ) represents the wavelength, (c) is the speed of a wave, (ϕ) varies in the range $(0 \le \phi \le \pi)$, when the value of $\phi = 0$ the channel is symmetric with waves out of phase and $\phi = \pi$ waves are in phase the rectangular coordinates has been designed in such a method that $\bar{X} - axis$ is along the path that waves use for propagation and $\bar{Y} - axis$ perpendicular to $\bar{X}$, $\bar{t}$ represents the time.

Further a_1, a_2, d, d' and ϕ satisfy the following condition

$$a_1^2 + a_2^2 + 2a_1a_2\cos\phi \le (d + d')^2 . \quad 3$$

Basic equation

The additional stress tensor for the Sutterby model is determined by [19 16]:

$$\bar{S} = \frac{\mu}{2}\left[\frac{\sinh^{-1}(n\dot{\gamma})}{n\dot{\gamma}}\right]^{m^*} A_1 \quad 4$$

$$\dot{\gamma} = \sqrt{\frac{1}{2}\text{tras}(A_1)^2} \quad 5$$

$$A_1 = \nabla\bar{V} + (\nabla\bar{V})^T \quad 6$$

Where $\bar{S}$ denotes the stress of the extra tensor, n, and m^* represents the material constants of the Sutterby fluid, $\nabla = (\partial\bar{X}, \partial\bar{Y}, 0)$ is the gradient vector, μ represents the dynamic viscosity and A_1 represents the first Rivilin–Ericksen tensor. The phrase $\sinh^{-1}$ is approximately equivalent to

$$\sinh^{-1}\left(\frac{\dot{\gamma}}{n}\right) = \frac{\dot{\gamma}}{n} - \frac{\dot{\gamma}^3}{6n^3} \quad 7$$

The constituents of the extra stress tensor of Sutterby defined by Eq 4 are listed below:

$$\bar{S}_{\bar{X}\bar{X}} = \frac{\mu}{2}[1 - \frac{mn^2}{6}\left(2\bar{U}_{\bar{X}}{}^2 + (\bar{V}_{\bar{X}} + \bar{U}_{\bar{Y}})^2 + 2\bar{V}_Y{}^2\right)]2\bar{U}_{\bar{X}} \quad 8$$

$$\bar{S}_{\bar{X}\bar{Y}} = \frac{\mu}{2}\left[1 - \frac{mn^2}{6}\left(2\bar{U}_{\bar{X}}{}^2 + (\bar{V}_{\bar{X}} + \bar{U}_{\bar{Y}})^2 + 2\bar{V}_Y{}^2\right)\right](\bar{U}_{\bar{X}} + \bar{V}_{\bar{Y}}). \quad 9$$

$$\bar{S}_{\bar{Y}\bar{Y}} = \frac{\mu}{2}\left[1 - \frac{mn^2}{6}\left(2\bar{U}_{\bar{X}}{}^2 + (\bar{V}_{\bar{X}} + \bar{U}_{\bar{Y}})^2 + 2\bar{V}_Y{}^2\right)\right]2\bar{V}_{\bar{Y}} \quad 10$$

2024, 21(5): 1625-1638
https://dx.doi.org/10.21123/bsj.2023.8312
P-ISSN: 2078-8665 - E-ISSN: 2411-7986
Baghdad Science Journal

The governing equation

The flow is controlled by three coupled nonlinear partial differentials of continuity, momentum, and energy, the governing equations in frame $(\bar{X}, \bar{Y})$ can be written as follows:

$$\frac{\partial \bar{U}}{\partial \bar{X}} + \frac{\partial \bar{V}}{\partial \bar{Y}} = 0 \quad 11$$

$$\rho\left(\frac{\partial \bar{U}}{\partial \bar{t}} + \bar{U}\frac{\partial \bar{U}}{\partial \bar{X}} + \bar{V}\frac{\partial \bar{U}}{\partial \bar{Y}}\right) - \rho\Omega\left(\Omega\bar{U} + 2\frac{\partial \bar{V}}{\partial \bar{t}}\right) = -\frac{\partial \bar{P}}{\partial \bar{X}} + \frac{\partial \bar{S}_{\bar{X}\bar{X}}}{\partial \bar{X}} + \frac{\partial \bar{S}_{\bar{X}\bar{Y}}}{\partial \bar{Y}} - \frac{\sigma {B_0}^2}{(1+m^2)}(\bar{U} - m\bar{V}) + g\rho\beta_T(T - T_0) - \frac{\mu}{k_0}\bar{U} + \rho g \sin\alpha. \quad 12$$

$$\rho\left(\frac{\partial \bar{V}}{\partial \bar{t}} + \bar{U}\frac{\partial \bar{V}}{\partial \bar{X}} + \bar{V}\frac{\partial \bar{V}}{\partial \bar{Y}}\right) - \rho\Omega\left(\Omega\bar{V} - 2\frac{\partial \bar{U}}{\partial \bar{t}}\right) = -\frac{\partial \bar{P}}{\partial \bar{Y}} + \frac{\partial \bar{S}_{\bar{X}\bar{Y}}}{\partial \bar{X}} + \frac{\partial \bar{S}_{\bar{Y}\bar{Y}}}{\partial \bar{Y}} - \frac{\sigma {B_0}^2}{(1+m^2)}(\bar{V} + m\bar{U}) - \frac{\mu}{k_0}\bar{V} + \rho g \cos\alpha. \quad 13$$

$$\rho C_P\left(\frac{\partial}{\partial \bar{t}} + \bar{U}\frac{\partial}{\partial \bar{X}} + \bar{V}\frac{\partial}{\partial \bar{Y}}\right)\bar{T} = k\left(\frac{\partial^2}{\partial \bar{t}^2} + \frac{\partial^2}{\partial \bar{X}^2} + \frac{\partial^2}{\partial \bar{Y}^2}\right)\bar{T} + \varphi_0 \quad 14$$

Where ρ is the fluid density, $(\bar{U}, \bar{V})$ the velocity components, $\bar{P}$ represents the hydrodynamic pressure, $\bar{S}_{\bar{X}\bar{X}}, \bar{S}_{\bar{X}\bar{Y}},$ and $\bar{S}_{\bar{Y}\bar{Y}}$ are the constituents of the extra stress tensor $\bar{S}$. σ is the electrical conductivity, φ_0 is the steady heat addition/absorption, B_0 is an applied magnetic field, β_T is the thermal expansion coefficient, g is the gravitational acceleration and Ω represents the rotation. The specific heat is denoted by C_P, α is the channel's angle of inclination with respect to the horizontal axis, k_0 material constant, the thermal conductivity by k, and the temperature by $\bar{T}$.

Peristaltic movement in reality is an unstable behavior, but it can be considered to be steady via The change from the experimental frame (fixed frame) $(\bar{X}, \bar{Y})$ to the wave frame (move frame) $(\bar{x}, \bar{y})$. The following transformations establish the link between coordinates, velocities, and pressure in laboratory frame $(\bar{X}, \bar{Y})$ to wave frame $(\bar{x}, \bar{y})$:

$$\bar{X} = \bar{x} - c\bar{t}\ , \bar{Y} = \bar{y}\ , \bar{U} = \bar{u} - c\ , \bar{V} = v\ , \bar{P}(\bar{x}, \bar{y}) = \bar{p}(\bar{X}, \bar{Y}, \bar{t}) \quad 15$$

Where $\bar{u}$ and $\bar{v}$ represent the components of velocity, and $\bar{p}$ denotes the pressure in the wave frame. Now, Eqs 15 will be substituted into Eqs. 1,. 2 and 11-**Error! Reference source not found.** and then normalize the equation that is produced by doing so by utilizing the non-dimensional quantities that are listed below:

$$x = \frac{1}{\lambda}\bar{x},\ y = \frac{1}{d}\bar{y},\ u = \frac{1}{c}\bar{u},\ v = \frac{1}{c}\bar{v},\ p = \frac{d^2}{\lambda\,\mu\,c}\bar{p},\ t = \frac{c}{\lambda}\bar{t},\ h_1 = \frac{1}{d}\overline{h_1},\ h_2 = \frac{1}{d}\overline{h_2},\ \delta = \frac{d}{\lambda},\ Re = \frac{\rho\,c\,d}{\mu},\ \bar{T} = T - T_0,\ \theta = \frac{T-T_0}{T_1-T_0},\ S_{ij} = \frac{d}{\mu\,c}\bar{S}_{\bar{i}\,\bar{j}},\ Gr = \frac{g\beta_T(T-T_0)d^2}{\mu c},\ Pr = \frac{\mu c_p}{k},\ \mathrm{Fr} = \frac{c^2}{gd},\ Da = \frac{k_0}{d^2}. \quad 16$$

Where, (δ) represents the wave number, (h_1) and (h_2) are the nondimensional upper and lower wall surface respectively, (Re) represents the Reynolds number, (Pr) represents the Prandtl number, (Gr) represents the Grashof number, (Fr) represents the Froude number, (M) represents the Hartman number, (Da) represents Darcy number, (Φ) represents the face difference,(A) represents the parameter of Sutterby liquid, and (T_0) and (T_1) are the wall temperatures at the top and bottom, respectively. Then, in view of Eqs.16, . 1,. 2, and 8 14 take the form:

$$h_1(x) = 1 + a\ sin\ x. \quad 17$$

$$h_2(x) = -d_1 - b\ \ sin\ (x\ + \phi). \quad 18$$

$$\delta\frac{\partial u}{\partial x} + \frac{\partial v}{\partial y} = 0. \quad 19$$

$$Re\left(\delta\frac{\partial u}{\partial t} + \delta u\frac{\partial u}{\partial x} + v\frac{\partial u}{\partial y}\right) - \frac{\rho d^2}{\mu}\Omega\left(\Omega u + 2\delta\frac{\partial v}{\partial t}\right) = -\frac{\partial p}{\partial x} + \delta\frac{\partial s_{xx}}{\partial x} + \frac{\partial \bar{S}_{xy}}{\partial y} - \frac{\sigma {B_0}^2}{(1+m^2)}(u - mv) + Gr\ \theta - \frac{1}{Da}u + \frac{Re}{Fr}\sin\alpha. \quad 20$$

$$Re\delta\left(\delta\frac{\partial v}{\partial t} + \delta u\frac{\partial v}{\partial x} + v\frac{\partial v}{\partial y}\right) - Re\frac{d}{c}\Omega\left(-\Omega\delta^2 v - 2\delta^2\frac{\partial u}{\partial t}\right) = -\frac{\partial p}{\partial y} + \delta^2\frac{\partial s_{xy}}{\partial x} + \delta\frac{\partial s_{yy}}{\partial y} - \frac{\sigma {B_0}^2}{(1+m^2)}\frac{d^2}{\mu}\delta(v + mu) - \frac{1}{Da}v + \frac{Re}{Fr}\cos\alpha. \quad 21$$

$$RePr\delta\left(\frac{\partial}{\partial t} + u\frac{\partial}{\partial x} + v\frac{\partial}{\partial y}\right)\theta = \left(\delta^2\frac{c^2\partial^2}{\partial t^2} + \delta^2\frac{\partial^2}{\partial x^2} + \frac{\partial^2}{\partial y^2}\right)\theta + B. \quad 22$$

Introduction to fluid flow (ψ) through a relationship:

$$u = \psi_y\ , v = -\delta\psi_x\ . \quad 23$$

2024, 21(5): 1625-1638
https://dx.doi.org/10.21123/bsj.2023.8312
P-ISSN: 2078-8665 - E-ISSN: 2411-7986
Baghdad Science Journal

Substituted Eqs 23 in Eq $\delta\frac{\partial u}{\partial x}+\frac{\partial v}{\partial y}=0.19$ to Eq. 22 respectively,

$$\delta\frac{\partial \psi_y}{\partial x}-\delta\frac{\partial \psi_x}{\partial y}=0. \quad 24$$

$$Re\left(\delta\frac{\partial \psi_y}{\partial t}+\delta\psi_y\frac{\partial \psi_y}{\partial x}-\delta\psi_x\frac{\partial \psi_y}{\partial y}\right)-\frac{\rho d^2}{\mu}\Omega\left(\Omega\psi_y+2\delta\frac{\partial \psi_x}{\partial t}\right)=-\frac{\partial p}{\partial x}+\delta\frac{\partial s_{xx}}{\partial x}+\frac{\partial s_{xy}}{\partial y}-\frac{\sigma {B_0}^2}{(1+m^2)}(\psi_y+m\delta\psi_x)+\mathrm{Gr}\,\theta-\frac{1}{Da}\psi_y+\frac{Re}{Fr}\sin\alpha. \quad 25$$

$$Re\delta\left(\delta\frac{\partial v}{\partial t}+\delta\psi_y\frac{\partial v}{\partial x}+\delta^2\psi_x\frac{\partial \psi_x}{\partial y}\right)+Re\frac{d}{c}\Omega\left(\Omega\delta\psi_x-2\delta^2\frac{\partial \psi_y}{\partial t}\right)=-\frac{\partial p}{\partial y}+\delta^2\frac{\partial s_{xy}}{\partial x}+\delta\frac{\partial s_{yy}}{\partial y}+\frac{\sigma {B_0}^2}{(1+m^2)}\frac{d^2}{\mu}\delta^2(\psi_x+m\psi_y)-\frac{1}{Da}\delta\psi_x+\frac{Re}{Fr}\cos\alpha. \quad 26$$

$$RePr\delta\left(\frac{\partial}{\partial t}+\psi_y\frac{\partial}{\partial x}-\delta\psi_x\frac{\partial}{\partial y}\right)\theta=\left(\delta^2\frac{c^2\partial^2}{\partial t^2}+\delta^2\frac{\partial^2}{\partial x^2}+\frac{\partial^2}{\partial y^2}\right)\theta+B. \quad 27$$

When (Re and δ <<1), the Eqs. from . 25-
. 27 become in the form :

$$-\frac{\rho d^2}{\mu}\Omega^2\psi_y=-\frac{\partial p}{\partial x}+\frac{\partial s_{xy}}{\partial y}-\frac{M^2}{(1+m^2)}\psi_y+Gr\,\theta-\frac{1}{Da}\psi_y+\frac{Re}{Fr}\sin\alpha. \quad 28$$

$$-\frac{\partial p}{\partial y}=0. \quad 29$$

$$\frac{\partial^2\theta}{\partial y^2}+\mathrm{B}=0. \quad 30$$

While an additional stress tensor component takes the following form:

$$s_{xy}=\frac{\partial^2\psi}{2\partial y^2}-A\left(\frac{\partial^2\psi}{\partial y^2}\right)^3, s_{xx}=0, s_{yy}=0. \quad 31$$

Where $M=\sqrt{\frac{\sigma}{\mu}}B_0 d$ the Hartman number, $A=\frac{\boldsymbol{mb^2c^2}}{\boldsymbol{6d^2}}$ the Sutterby liquid parameter and $\mathrm{B}=\frac{d^2\theta}{k(T_1-T_0)}$ the constant heat radiation
If
Eq=0.
31 is substituted into Eq. 28 and the derivative with respect to y is taken, the following equation is obtained:

$$\frac{\partial^4\psi}{\partial y^4}\left[1-3A\left(\frac{\partial^2\psi}{\partial y^2}\right)^2\right]-6A\frac{\partial^2\psi}{\partial y^2}\left(\frac{\partial^3\psi}{\partial y^3}\right)^2+2(\frac{\rho d^2}{\mu}\Omega^2-\frac{M^2}{m^2+1}-\frac{1}{Da})\frac{\partial^2\psi}{\partial y^2}+2Gr\frac{\partial\theta}{\partial y}+\frac{Re}{Fr}\sin\alpha=0. \quad 32$$

$$\frac{\partial^2\theta}{\partial y^2}+B=0. \quad 33$$

In wave frames, the dimensionless boundary conditions are:

$$\psi=\frac{F}{2}, \frac{\partial\psi}{\partial y}=-1 \quad at\ y=h_1. \quad 34$$

$$\psi=\frac{-F}{2}, \frac{\partial\psi}{\partial y}=-1 \quad at\ y=h_2. \quad 35$$

$$\theta=0\ at\ y=h_1, \theta=1\ \ at\ y=h_2. \quad 36$$

Where F is just the flow rate, which is dimensionless in time in the frame of the wave. It is associated with the form that has no dimensions' temporal flow rate Q1 in the experimental frame via the expression:

$$Q_1=F+1+d. \quad 37$$

as a, b, Φ and d achieve Eq . 3:

$$a^2+b^2+2abcos(\Phi)\le(1+d_1)^2. \quad 38$$

Initially, the nonlinear equation Eq.

33 is solved by integrating and substituting the boundary conditions Eq..

36, and then the solution to Eq.37 is obtained:

$$\theta=-\frac{-2\mathrm{h}_1+\mathrm{h}_1^2\mathrm{h}_2B-\mathrm{h}_1\mathrm{h}_2^2B}{2(h_1-\mathrm{h}_2)}-\frac{(2-\mathrm{h}_1^2B+\mathrm{h}_2^2B)y}{2(\mathrm{h}_1-\mathrm{h}_2)}-\frac{By^2}{2}. \quad 39$$

By differentiating Eq. 39 with respect to y and substituting it into Eq. 32, now obtaining the following nonlinear equation:

$$\frac{\partial^4\psi}{\partial y^4}\left[1-3A\left(\frac{\partial^2\psi}{\partial y^2}\right)^2\right]-6A\frac{\partial^2\psi}{\partial y^2}\left(\frac{\partial^3\psi}{\partial y^3}\right)^2+2(\frac{\rho d^2}{\mu}\Omega^2-\frac{M^2}{m^2+1}-\frac{1}{Da})\frac{\partial^2\psi}{\partial y^2}+2Gr(-\frac{(2-\mathrm{h}_1^2B+\mathrm{h}_2^2B)}{2(\mathrm{h}_1-\mathrm{h}_2)}-\mathrm{By})=0. \quad 40$$

2024, 21(5): 1625-1638
https://dx.doi.org/10.21123/bsj.2023.8312
P-ISSN: 2078-8665 - E-ISSN: 2411-7986
Baghdad Science Journal

Solution of the problem

It is not possible to that construct a solution in closed form for each and every one of the arbitrary parameters involved in Equation Eq . 40, as it is highly non-linear and convoluted. Therefore, the perturbation approach is used to get the answer. The solution was expanded to include perturbation: [18]

$$\psi = \psi_0 + A\psi_1 + o(A^2). \quad 41$$

And by substituting Eq. 36 into Eqs. 28-. 33, along with the boundary conditions Eq . 34 and Eq . 35 and equating the coefficients of similar powers of A, The following system of equations is obtained:

1. Zeroth order system

When such terms of order (A) in a zero-order system are negligible, the result is

$$\psi_{0yyyy} + \zeta\psi_{0yy} - \gamma y + \eta = 0. \quad 42$$

Where $\zeta = 2(\frac{\rho d^2}{\mu}\Omega^2 - \frac{1}{Da} - \frac{M^2}{m^2+1})$.

$$\gamma = 2GrB.$$

And $\eta = Gr[B(h_1 + h_2) - \frac{2}{h_1 - h_2}]$.

Such that

$$\psi_0 = \frac{F_0}{2}, \frac{\partial\psi_0}{\partial y} = -1 \quad at \quad y = h_1. \quad 43$$

and

$$\psi_0 = \frac{-F_0}{2}, \frac{\partial\psi_0}{\partial y} = -1 \quad at \quad y = h_2. \quad 44$$

2. First order system

$$\psi_{1yyyy} + \zeta\psi_{1yy} = 3\psi_{0yyyy}(\psi_{0yy})^2 + 6\psi_{0yy}(\psi_{0yyy})^2. \quad 45$$

$$\psi_1 = \frac{F_1}{2}, \frac{\partial\psi_1}{\partial y} = 0 \quad at \quad y = h_1. \quad 46$$

and

$$\psi_1 = \frac{-F_1}{2}, \frac{\partial\psi_1}{\partial y} = 0 \quad at \quad y = h_2. \quad 47$$

Solving the relevant zeroth-order and first-order systems yields the final stream function equation.

$$\psi = \psi_0 + A\psi_1. \quad 48$$

Results and Discussion

This section consists of two subsections. Using Mathematica, the stream function is depicted in the first and the pressure gradient is presented in the second.

1. Trapping Phenomena

Trapping is another fascinating phenomenon of peristaltic motion. Essentially, it is the production of an internally circulating fluid bolus by means of a closed streamline. This captured bolus propelled the head along peristaltic waves. in Figs (a) (b) (c)

Figure 2**Error! Reference source not found.** Describes the effect of the parameters $\Omega, M, Gr, B, Da, m, A, \phi, and\ \alpha$ on stream function. As for Fig (a) (b) (c)

Figure 2, the trapped bolus size close to the upper wall increases but the trapped bolus size close to the lower wall decreases with an increase in the rotation (Ω). While Fig **Error! Reference source not found.** illustrates that the trapped bolus size close to the upper wall increases but the trapped bolus size close to the lower wall decreases with increasing the Hartmann number (M). With increasing the Thermal Grashof number (Gr), the size of the trapped bolus close to the lower wall decreases while the trapped bolus close to the upper wall doesn't change in Fig **Error! Reference source not found.**. In Fig **Error! Reference source not found.** the sizes of trapped boluses close to the upper and the lower wall decrease with increasing the constant heat radiation (B).**Error! Reference source not found.** shows that as the Darcy number (Da) goes up, the trapped bolus size close to the upper wall rises slightly but the trapped bolus size close to the

2024, 21(5): 1625-1638
https://dx.doi.org/10.21123/bsj.2023.8312
P-ISSN: 2078-8665 - E-ISSN: 2411-7986
Baghdad Science Journal

lower wall reduces slightly. **Error! Reference source not found.** illustrates a rise in the size of the trapped bolus close to the upper wall and goes down in the size of the trapped bolus close to the lower wall of a channel with increasing Hall parameter (m). The trapped bolus size close to the upper wall increases while the trapped bolus size close to the lower wall decreases with the increase of the fluid parameter (A) that is in Fig**Error! Reference source not found.**.While in **Error! Reference source not found.**, the trapped bolus size close to the upper wall decreasing but the trapped bolus size close to the lower wall increasing with the increase of the wavelength (ϕ).

2. Pressure gradient dp/dx:

Graphically, the influence that relevant parameters $\Omega, M, Gr, B, Re, Fr, Da, m, A, \phi \text{ and } \alpha$ have on the pressure gradient dp/dx can be seen in **Error! Reference source not found.**-Figure **10**. As seen in **Error! Reference source not found.**, increasing the rotation (Ω) results in an increasing pressure gradient. Figure 3 illustrates how increasing values of the Hartmann number (M) are associated with a diminishing pressure gradient. Increasing the thermal Grashof number (Gr) increases the pressure gradient in the left edge of the channel, but has no effect in the central region toward the right side of the channel wall, as depicted in **Error! Reference source not found.**. Figure 4 shows that as the constant heat radiation (B) goes up, the pressure gradient goes up toward the right edge of the channel wall but has no effect in the center and the left side of the channel wall. In **Error! Reference source not found.**, the pressure gradient has no change with the increasing Reynold number (Re). As shown in Figure 5, increasing the value of the Froude number (Fr) doesn't change the pressure gradient. Also, the pressure gradient doesn't change with the increasing of the Darcy number (Da) as clear in Figure 6. Figure 7 demonstrates that the pressure gradient grows as the Hall parameter value (m) increases. Figure 8 shows that the pressure gradient rises as the value of a fluid parameter (A) increases. Figure 9 displays, that the pressure gradient reduces in the middle towards the left wall gradually and then has no effect as the face difference (ϕ) increases whereas increases near the right wall. Figure 10, shows that the pressure gradient does not affect increasing of the channel's angle of inclination with respect to the horizontal axis(α).

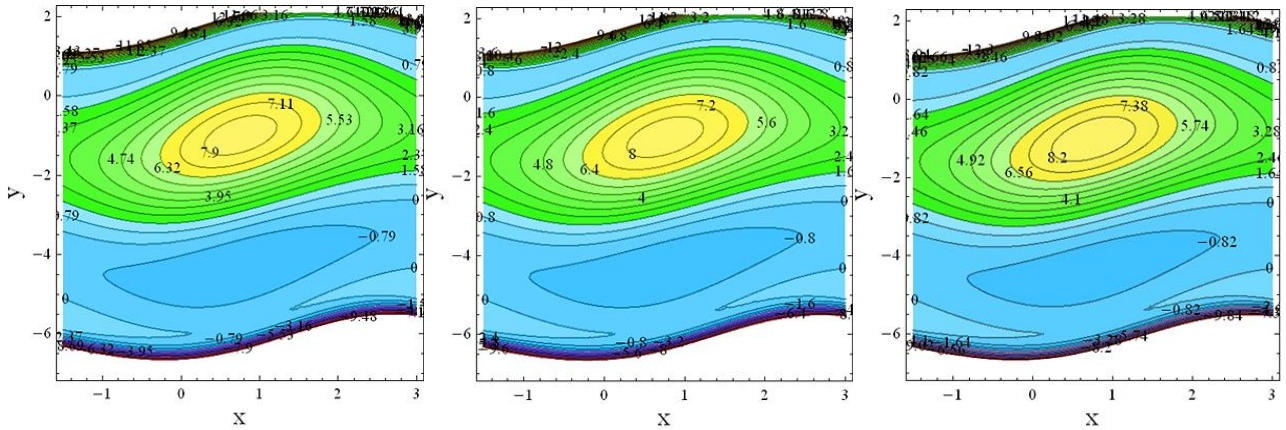

(a) (b) (c)

Figure 2. Distribution of streamlines for (a)Ω=0.5, (b)Ω=2.5, (c)Ω=4.5, M=5, Gr=5, B=0.5, Da=8, m=6.5, A=0.3, ϕ=1.5

2024, 21(5): 1625-1638
https://dx.doi.org/10.21123/bsj.2023.8312
P-ISSN: 2078-8665 - E-ISSN: 2411-7986
Baghdad Science Journal

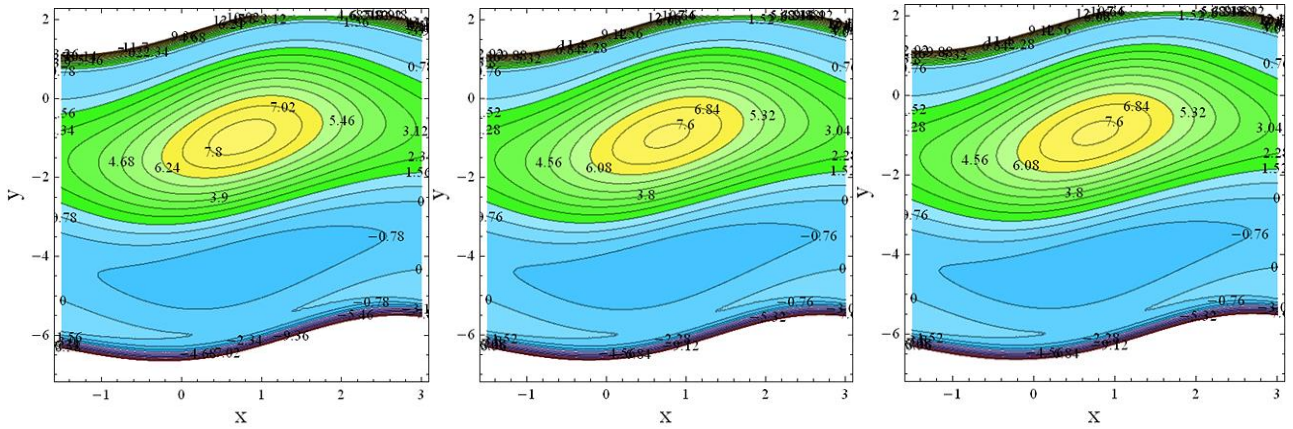

(a) (b) (c)

Figure 3. Distribution of streamlines for Ω=1, (a)M=5.1, (b)M=5.2, (c)M=5, Gr=5, B=0.5, Da=8, m=6.5, A=0.3, ϕ1.5

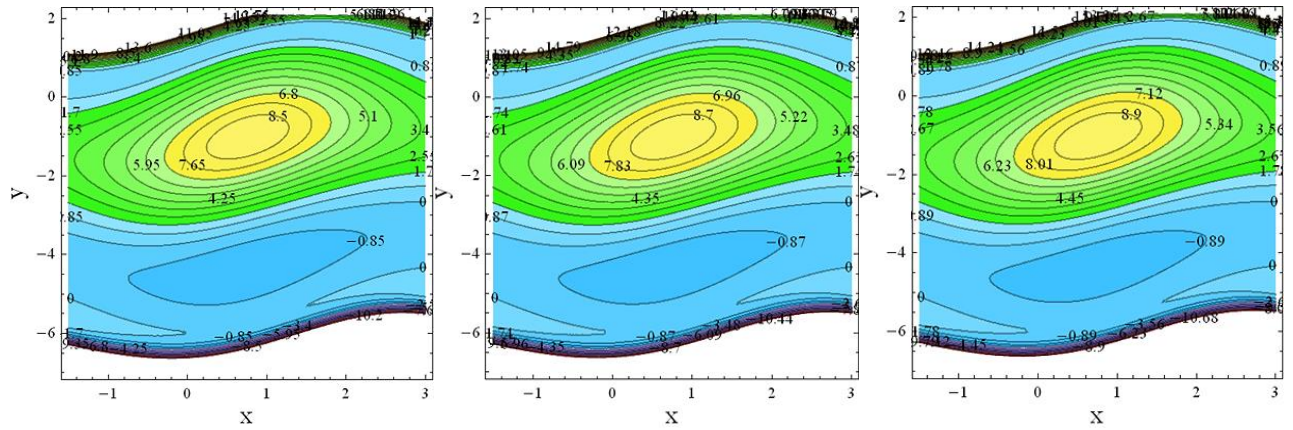

(a) (b) (c)

Figure 4. Distribution of streamlines for Ω=1, M=5, (a)Gr=5.3, (b)Gr=5.4, (c)Gr=5.5, B=0.5, Da=8, m=6.5, A=0.3, ϕ=1.5

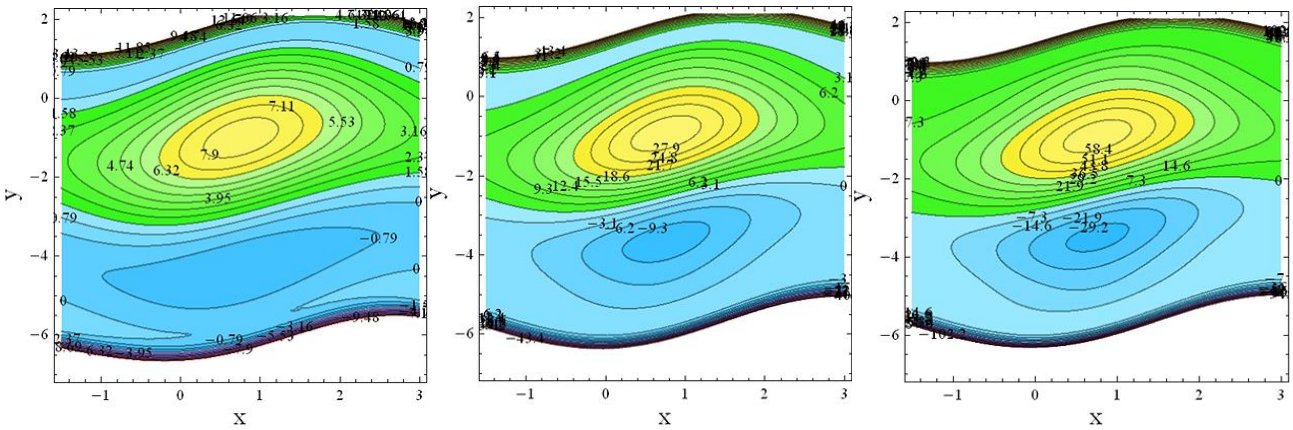

(a) (b) (c)

Figure 5. Distribution of streamlines for Ω=1, M=5, Gr=5, (a)B=0.5, (b)B=1.5, (c)B=2.5, Da=8, m=6.5, A=0.3, ϕ=1.5

2024, 21(5): 1625-1638
https://dx.doi.org/10.21123/bsj.2023.8312
P-ISSN: 2078-8665 - E-ISSN: 2411-7986
Baghdad Science Journal

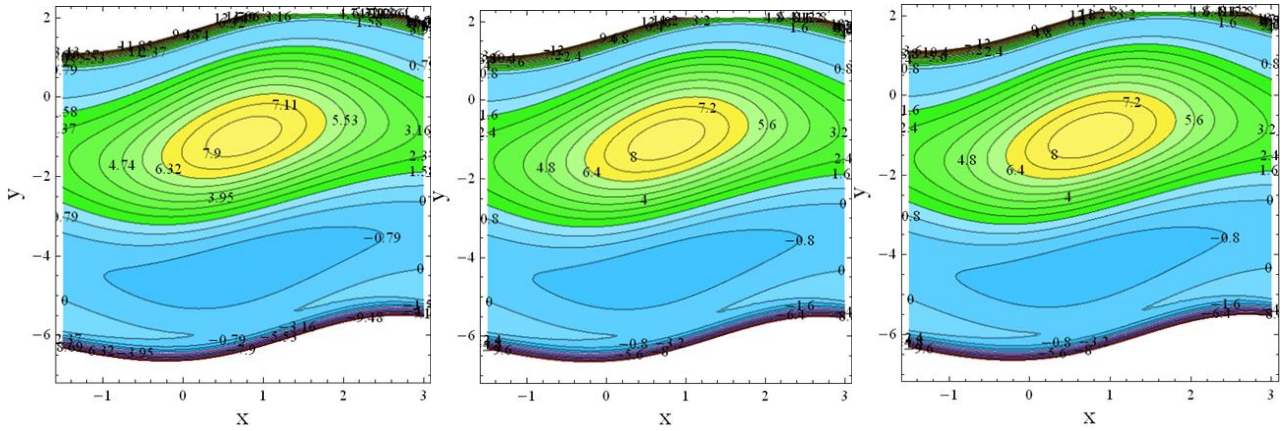

(a) (b) (c)

Figure 6. Distribution of streamlines for Ω=1, M=5, Gr=5, B=0.5, (a)Da=8, (b)Da=9, (c)Da=10, m=6.5, A=0.3, ϕ=1.5

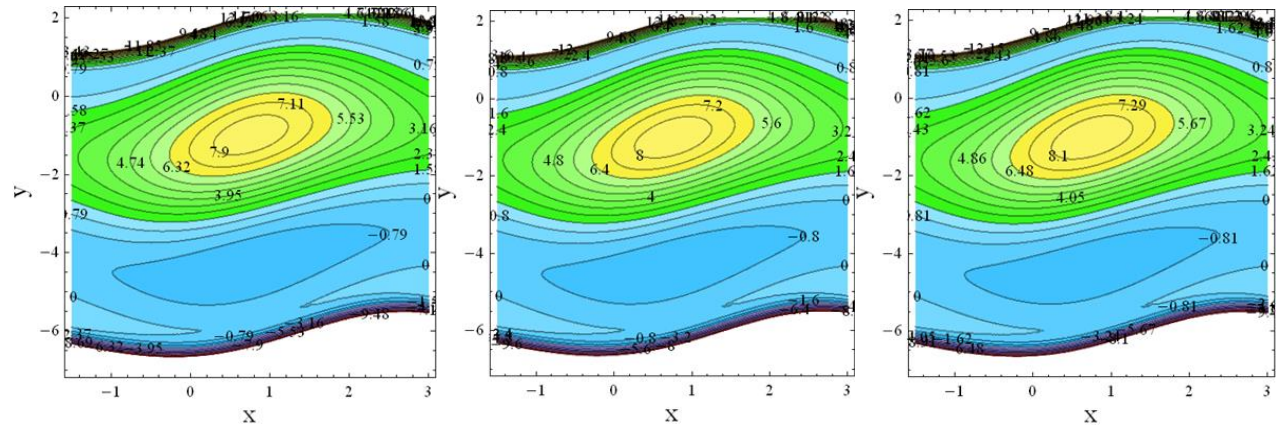

(a) (b) (c)

Figure 7. Distribution of streamlines for Ω=1, M=5, Gr=5, B=0.5, Da=8, (a)m=6.5, (b)m=6.6, (c)m=6.7, A=0.3, ϕ=1.5

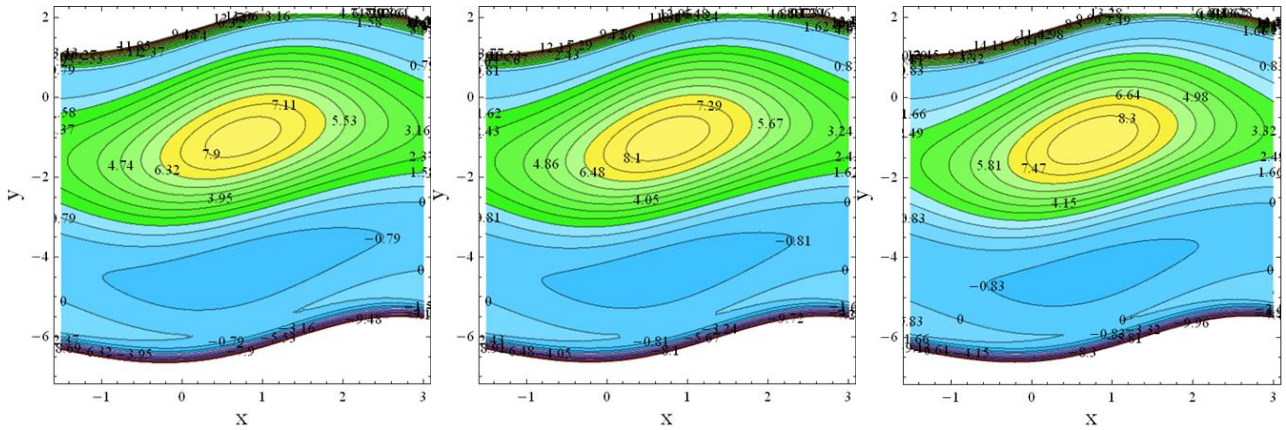

(a) (b) (c)

Figure 8. Distribution of streamlines for Ω=1, M=5, Gr=5, B=0.5, Da=8, m=6.5, (a)A=0.3, (b)A=0.35, (c)A=0.4, ϕ=1.5

2024, 21(5): 1625-1638
https://dx.doi.org/10.21123/bsj.2023.8312
P-ISSN: 2078-8665 - E-ISSN: 2411-7986
Baghdad Science Journal

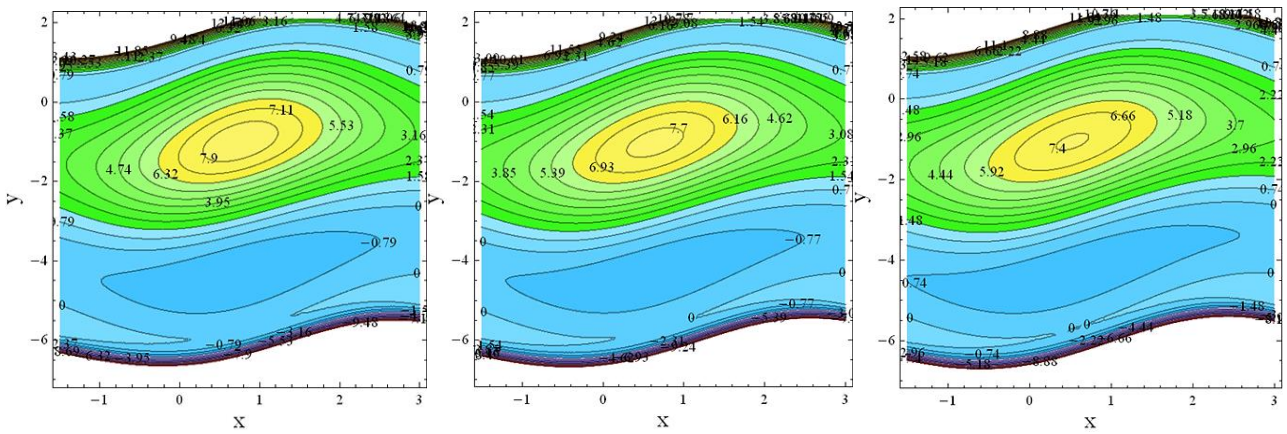

(a) (b) (c)

Figure 9. Distribution of streamlines for Ω=1, M=5, Gr=5, B=0.5, Da=8, m=6.5, A=0.3, (a)ϕ=1.5, (b)ϕ=1.7, (c)ϕ=1.9

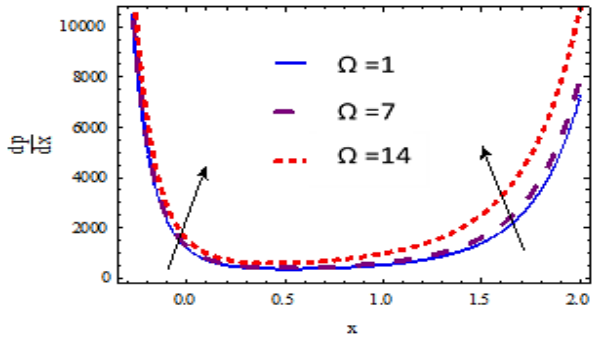

Figure 10. Pressure gradient and variation for different of Ω when M=5, Gr=1, B=0.08, Re=0.2, Fr=0.2, Da=8, m=7, A=5, ϕ=Pi/6, α=0.5

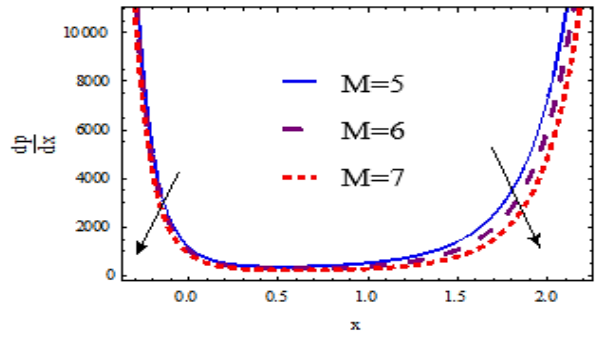

Figure 3. Pressure gradient and variation for different of M when Ω=1, Gr=1, B=0.08, Re=0.2, Fr=0.2, Da=8, m=7, A=5, ϕ=Pi/6, α=0.5

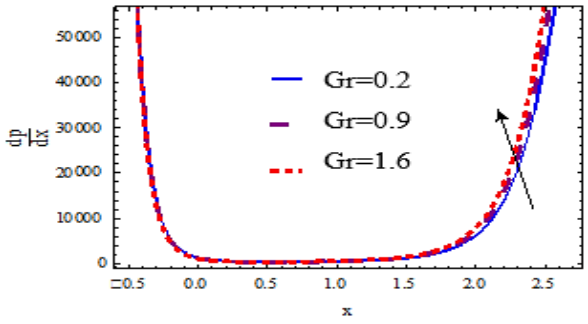

Figure 12. Pressure gradient and variation for different of Gr when Ω=1, M=5, B=0.08, Re=0.2, Fr=0.2, Da=8, m=7, A=5, ϕ=Pi/6, α=0.5

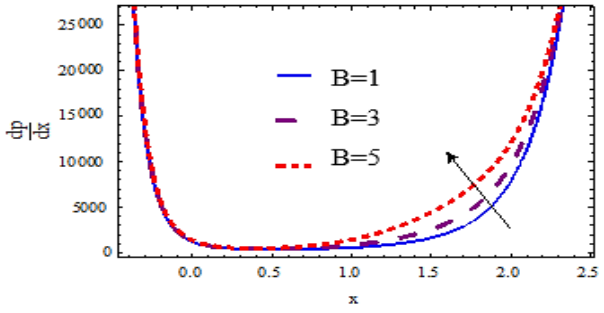

Figure 4. Pressure gradient and variation for different of B when Ω=1, M=5, Gr=1, Re=0.2, Fr=0.2, Da=8, m=7, A=5, ϕ=Pi/6, α=0.5

2024, 21(5): 1625-1638
https://dx.doi.org/10.21123/bsj.2023.8312
P-ISSN: 2078-8665 - E-ISSN: 2411-7986
Baghdad Science Journal

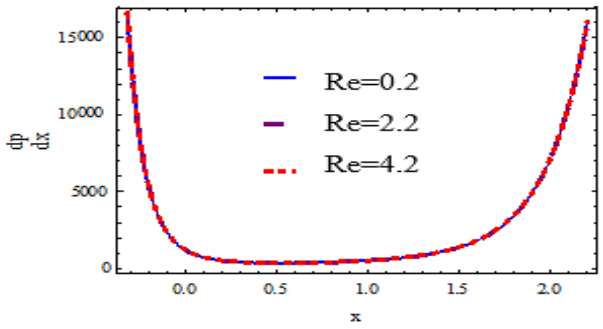

Figure 14. Pressure gradient and variation for different of Re when Ω=1, M=5, Gr=1, B=0.08, Fr=0.2, Da=8, m=7, A=5, ϕ=Pi/6, α=0.5

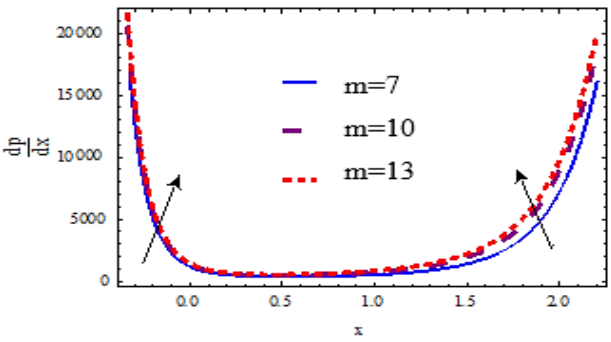

Figure 7. Pressure gradient and variation for different of m when Ω=1, M=5, Gr=1, B=0.08, Re=0.2, Fr=0.2, Da=8, A=5, ϕ=Pi/6, α=0.5

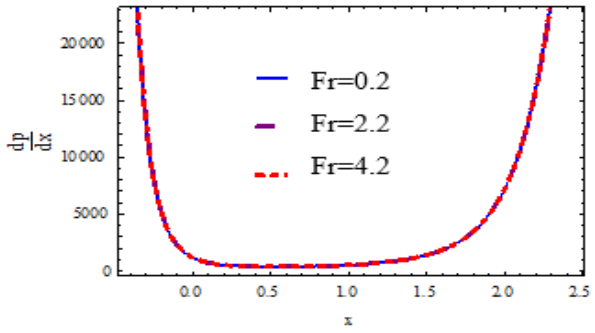

Figure 5. Pressure gradient and variation for different of Fr when Ω=1, M=5, Gr=1, B=0.08, Re=0.2, Da=8, m=7, A=5, ϕ=Pi/6, α=0.5

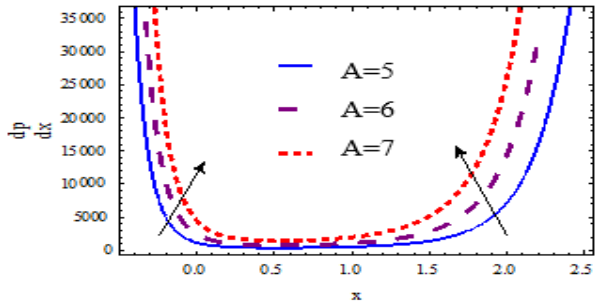

Figure 8. Pressure gradient and variation for different of A when Ω=1, M=5, Gr=1, B=0.08, Re=0.2, Fr=0.2, Da=8, m=7, ϕ=Pi/6, α=0.5

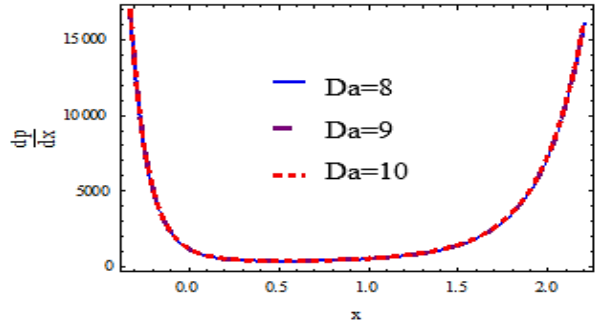

Figure 6. Pressure gradient and variation for different of Da when Ω=1, M=5, Gr=1, B=0.08, Re=0.2, Fr=0.2, m=7, A=5, ϕ=Pi/6, α=0.5

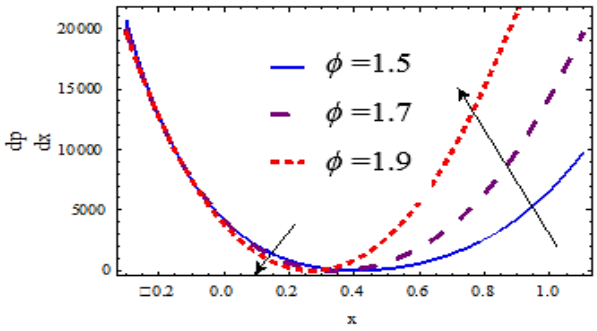

Figure 9. Pressure gradient and variation for different of ϕ when Ω=1, M=5, Gr=1, B=0.08, Re=0.2, Fr=0.2, Da=8, m=7, A=5, α=0.5

2024, 21(5): 1625-1638
https://dx.doi.org/10.21123/bsj.2023.8312
P-ISSN: 2078-8665 - E-ISSN: 2411-7986
Baghdad Science Journal

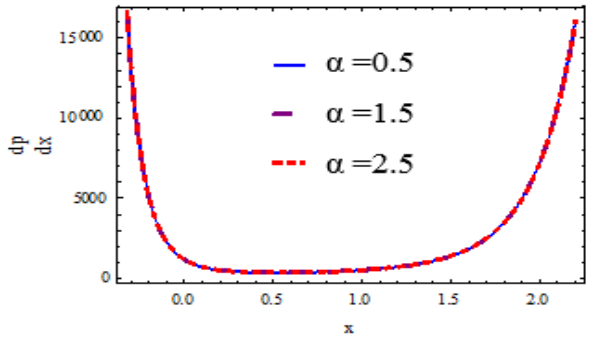

Figure 10. Pressure gradient and variation for different of α when Ω=1, M=5, Gr=1, B=0.08, Re=0.2, Fr=0.2, Da=8, m=7, A=5, ϕ=pi/6

Conclusion

In this article, the influence of heat transfer and rotation on a Sutterby fluid in an asymmetric channel was investigated. In this investigation, a lot of attention has been paid to the analysis of things like stream function and pressure gradient based on a simple analytical solution. The key findings of the current research are summarized below:

- ✓ The trapped bolus size close to the upper wall increases but the trapped bolus size close to the lower wall decreases with an increase in (Ω), (Da), (m), and (A).
- ✓ The trapped bolus size close to the upper wall increases but the trapped bolus size close to the lower wall decreases with increasing (M) and (ϕ).
- ✓ With increasing (Gr), the trapped bolus size close to the lower wall decreases while the trapped bolus close to the upper wall doesn't change.
- ✓ The sizes of trapped boluses close to the upper and the lower wall decrease with increasing constant heat radiation (B).
- ✓ Increasing (Ω), (m) and (A) results in an increasing the pressure gradient.
- ✓ The increasing value of (M) is associated with a diminishing pressure gradient.
- ✓ As (Gr) and (B) goes up, the pressure gradient goes up toward the right edge of the channel wall but has no effect in the center and the left side of the channel wall.
- ✓ The pressure gradient has no change with the increasing of (Re), (Fr), (Da), and (α).
- ✓ The pressure gradient grows as (m) increases.
- ✓ The pressure gradient reduces in the middle towards the left wall gradually and then has no effect as the face difference (ϕ) increases whereas increases near the right wall.

Authors' Declaration

- Conflicts of Interest: None.
- We hereby confirm that all the Figures and Tables in the manuscript are ours. Furthermore, any Figures and images, that are not ours, have been included with the necessary permission for re-publication, which is attached to the manuscript.
- Ethical Clearance: The project was approved by the local ethical committee in University of Baghdad.

Authors' Contribution Statement

This work was carried out in collaboration between all authors. A. A. M. and L. Z. H. read and approved the final manuscript.

References

1. Mohaisen HN, Abedulhadi AM. Effects of the Rotation on the Mixed Convection Heat Transfer Analysis for

the Peristaltic Transport of Viscoplastic Fluid in Asymmetric Channel. Iraqi J Sci. 2022; 63(3): 1240–1257. https://doi.org/10.24996/ijs.2022.63.3.29
2. Hayat T, Ayub S, Alsaedi A, Tanveer A, Ahmad B. Numerical simulation for peristaltic activity of Sutterby fluid with modified Darcy's law. Results Phys. 2017; 7: 762–768. https://doi.org/10.1016/j.rinp.2017.01.038
3. Latham TW. Fluid motions in a peristaltic pump. M Sc Thesis; Massachusetts Institute of Technology. Department of Mechanical Engineering. 1966. http://hdl.handle.net/1721.1/17282
4. Shapiro AH, Jaffrin MY, Weinberg SL. Peristaltic pumping with long wavelengths at low Reynolds number. J Fluid Mech. 1969; 37(4): 799–825. https://doi.org/10.1017/S0022112069000899
5. Kareem RS, Abdulhadi AM. Impacts of Heat and Mass Transfer on Magneto Hydrodynamic Peristaltic Flow Having Temperature-dependent Properties in an Inclined Channel Through Porous Media. Iraqi J Sci. 2020; 61(4): 854–869. https://doi.org/10.24996/ijs.2020.61.4.19
6. Nazeer M, Irfan M, Hussain F, Siddique I, Khan MI, Guedri K, et al. Analytical study of heat transfer rate of peristaltic flow in asymmetric channel with laser and magnetic effects: Remedy for autoimmune disease. Int J Mod Phys B. 2022; 37(3): 47-65. https://doi.org/10.1142/S021797922350025X
7. Ali HA. Impact of Varying Viscosity with Hall Current on Peristaltic Flow of Viscoelastic Fluid Through Porous Medium in Irregular Microchannel. Iraqi J Sci. 2022; 63(3): 1265–1276. https://doi.org/10.24996/ijs.2022.63.3.31
8. Nassief AM, Murad MA. The influence of magnetohydrodynamic flow and slip condition on generalized Burgers' fluid with fractional derivative. Baghdad Sci J. 2020; 17(1): 150-158. https://doi.org/10.21123/bsj.2020.17.1.0150
9. Abdulhadi AM, Ahmed TS. Effect of magnetic field on peristaltic flow of Walters' B fluid through a porous medium in a tapered asymmetric channel. J Adv Math. 2017; 12(1): 6889–6893. https://doi.org/10.24297/jam.v12i12.4440
10. Sadaf H, Akbar MU, Nadeem S. Induced magnetic field analysis for the peristaltic transport of non-Newtonian nanofluid in an annulus. Math Comput Simul. 2018; 148: 16–36. https://doi.org/10.1016/j.matcom.2017.12.009
11. Sutterby JL. Laminar converging flow of dilute polymer solutions in conical sections: Part I. Viscosity data, new viscosity model, tube flow solution. Am Inst Chem Eng. 1966; 12(1): 63–68. https://doi.org/10.1002/aic.690120114
12. Hayat T, Nisar Z, Alsaedi A, Ahmad B. Analysis of activation energy and entropy generation in mixed convective peristaltic transport of Sutterby nanofluid. J Therm Anal Calorim. 2021; 143(3): 1867–1880. https://doi.org/10.1007/s10973-020-09969-1
13. Alshareef TS. Impress of rotation and an inclined MHD on waveform motion of the non-Newtonian fluid through porous canal. J Phys Conf Ser. IOP Publishing. 2020; 1591(1): 12061. https://doi.org/10.1088/1742-6596/1591/1/012061
14. Kalyani K, Mvvnl SR. A Numerical Study on Cross Diffusion Cattaneo-Christov Impacts of MHD Micropolar Fluid Across a Paraboloid. Iraqi J Sci. 2021; 62(4): 1238–1264. https://doi.org/10.24996/ijs.2021.62.4.20
15. Khudair WS, Dwail HH. Studying the magnetohydrodynamics for williamson fluid with varying temperature and concentration in an inclined channel with variable viscosity. Baghdad Sci J. 2021; 18(3): 531-538. https://doi.org/10.21123/bsj.2021.18.3.0531
16. Ahmad S, Farooq M, Javed M, Anjum A. Double stratification effects in chemically reactive squeezed Sutterby fluid flow with thermal radiation and mixed convection. Results Phys. 2018; 8: 1250–1259. https://doi.org/10.1016/j.rinp.2018.01.043
17. Ramesh K, Prakash J. Thermal analysis for heat transfer enhancement in electroosmosis-modulated peristaltic transport of Sutterby nanofluids in a microfluidic vessel. J Therm Anal Calorim. 2019; 138(2): 1311–1326. https://doi.org/10.1007/s10973-018-7939-7
18. Atlas F, Javed M, Imran N. Effects of heat and mass transfer on the peristaltic motion of Sutterby fluid in an inclined channel. Multidiscip. Model Mater Struct 2020; 16(6): 1357–1372. https://www.emerald.com/insight/content/doi/10.1108/MMMS-08-2019-0156/full/html
19. Abdulla SA, Hummady LZ. Inclined magnetic field and heat transfer of asymmetric and porous medium channel on hyperbolic tangent peristaltic flow. Int J Nonlinear Anal Appl. 2021; 12(2): 2359–2373. http://dx.doi.org/10.22075/ijnaa.2021.5382

2024, 21(5): 1625-1638
https://dx.doi.org/10.21123/bsj.2023.8312
P-ISSN: 2078-8665 - E-ISSN: 2411-7986
Baghdad Science Journal

تأثير الانتقال الحراري والدوران على التدفق التمعجي لسائل سوتربي في قناة مائلة وغير متماثلة ذات مسامية

أسماء عبد الحسين محمد[2,1]، لقاء زكي حمادي[1]

قسم الرياضات، كلية العلوم، جامعة بغداد، بغداد، العراق.
قسم الرياضات، كلية العلوم للبنات، جامعة بغداد، بغداد، العراق.

الخلاصة

في هذا البحث تم دراسة تأثير متغير الدوران والمتغيرات الأخرى على التدفق التمعجي لسائل سوتربي في قناة غير متماثلة مائلة تحتوي على وسط مسامي مع انتقال الحرارة. في وجود الدوران، تم تطوير النمذجة الرياضية باستخدام المعادلات الاساسية القائمة على نموذج سائل سوتربي. في تحليل التدفق، يتم استخدام افتراضات مثل تقريب طول الموجة الطويلة وانخفاض عدد رينولدز. تم حل المعادلة التفاضلية الاعتيادية غير الخطية الناتجة تحليلياً باستخدام طريقة الاضطراب. يتم تحليل تأثيرات رقم كراشوف، ورقم هارتمان، ورقم رينولد، ورقم فرود، ومعلمة هال، ورقم دارسي، والمجال المغناطيسي، ومعلمة سائل سوتربي، وتحليل نقل الحرارة على وظيفة التدفق وتدرج الضغط بيانياً. باستخدام برنامج ماثيماتيكا، تم حساب النتائج العددية. تم اكتشاف أن حجم الفقاعات يتناقص مع زيادة بعض المعلمات ، بينما يتناسب تدرج الضغط تناسب طردي مع غالبية المعلمات.

الكلمات المفتاحية: انتقال الحرارة، المجال المغناطيسي، التدفق التمعجي، المسامية، سائل سوتربي.